Understanding the Brain Injury Mechanisms of Primary Blast Exposure

Karin A. Rafaels, Ann Mae DiLeonardi, Cameron R. Bass

Abstract Blast brain injury research has largely focused on the pressure transmission of the blast wave to the head. However, the large dynamic pressures can also cause high head accelerations. The injury mechanisms and sequelae from shock waves and head accelerations may not be the same, but both may be significant contributors to the overall pathology. In this study, we examine two immunohistochemical markers of axonal injury from blast exposures with varying head accelerations to anaesthetised ferrets. The immunohistochemical marker for neurofilament compaction, RM014 stained approximately 1,000 times more tissue area than the marker for impaired axonal transport, β-APP. .This trend in positive reactivity was most apparent in the large white matter tracts. The positive relationships between their immunoreactivities and impulse were similar, but RM014 had a slightly greater dependence on head acceleration than β-APP. Another observation was that the positive staining for the two axonal injury markers did not always occur in the same anatomical regions. The different injury patterns witnessed for the two markers highlight the complexity of blast brain injury compared with blunt neurotrauma. This study demonstrates that the accelerative aspect of the exposure event may contribute to the injury outcome.

Keywords Blast brain injury, head, acceleration, ferret, immunohistochemistry.

I. INTRODUCTION

Blast injuries are grouped into categories based on their underlying mechanisms [1-2]. Primary blast injuries result from the direct effects of the pressure wave and are a unique mechanism in blast events. Consequently, most of the research into blast brain injury has focused on the pressure transmission of the blast wave to the head [3-9]. However, in addition to direct transmission of the stress waves to the brain tissue, the large dynamic pressures of the blast event can also cause high head accelerations. The injury mechanisms and sequelae for shock wave-induced injury and accelerative-induced injury may not be the same, but both may be significant contributors to the overall pathology [10-11].

Axonal injury is a common pathology of traumatic brain injury (TBI) [12] that has also been demonstrated in models of blast injury [6][13-20]. Axons are believed to be especially vulnerable to mechanical loading because they span different areas of the brain, crossing the grey-white matter interface, running along ventricles or near blood vessels, which can create stress concentrations at these boundaries [21]. To support their length, axons are packed with parallel arrays of neurofilaments and microtubules that provide structural stability and a means to rapidly convey materials back and forth between the cell body and the axon terminus [22]. However, when exposed to a mechanical load, it is often a secondary, subsequent response that leads to morphological and structural changes in the cytoskeletal network [23-30]. Though all of the axons in a given region should be subjected to similar loading conditions, not all of the axons undergo the same structural changes [31-32].

Immunohistochemical (IHC) techniques provide a window into the biochemical pathways that can cause damage after the initial insult has occurred and that are otherwise difficult to investigate. Conformational changes to the neurofilaments in the axonal cytoskeleton have already been demonstrated after primary blast exposure using IHC of neurofilaments [18][33-34]. Microtubule damage was also identified after primary blast exposure via IHC methods to visualise impaired axonal transport [17][18][33][35]. Although, both major components of axonal cytoskeleton can be damaged after blast exposure, the two injury sequelae often do not occur in the same axons in traditional TBI [31-32]. Limited evidence for blast brain injury also suggest that neurofilament damage and

K. A. Rafaels (e-mail: karin.a.rafaels.civ@mail.mil; tel: +1-410-278-9459) is a Biomedical Engineer in the Warfighter Survivability Branch of the Survivability and Lethality Analysis Directorate. A. M. DiLeonardi is a Neuroscientist in the Soldier Protection Sciences Branch of the Weapons and Materials Research Directorate of the Army Research Laboratory. C. R. Bass is an Associate Research Professor in the Department of Biomedical Engineering at Duke University.

microtubule disruption may not be co-localised [34]. These differences in cytoskeletal changes may suggest separate underlying mechanisms of injury. Since primary blast has two major potential loading pathways, there may be differences in the injury patterns of axonal cytoskeletal injury between the injury mechanisms.

The objective of this study is to investigate the histologic differences between blast exposures with varying head accelerations. RM014 was selected to investigate neurofilament damage because it exclusively binds to the rod domain of the neurofilament medium chain only when there has been a side-arm modification or loss [36-37]. β-amyloid precursor protein (β-APP)-immunoreactivity, one of the most sensitive markers in traditional traumatic axonal injury, was selected to identify impaired axonal transport [38-39]. Moreover, both of these markers have reported immunoreactivity dependent on injury severity and at early time points post-injury [31][40-44]. We hypothesise that the amount of positive immunoreactivity is different for the two IHC labels, and that there is a different amount of positive staining for each marker depending on the magnitude of loading for the two injury mechanisms (shock wave and acceleration).

II. METHODS

Blast Brain Injury Model

A subset of the 64 male ferrets (*Mustela putorous furo*) from [45] were used in this histologic examination of blast brain injury. Histologic sections from seven of the ferrets that were exposed to similar peak overpressures and various levels of impulse and gross head accelerations were selected. Histology from one control animal (i.e. an animal that did not undergo a blast exposure) was also analysed. Table I provides the body mass, head geometry and blast test conditions for each ferret. The experimental protocol was approved by the University of Virginia Animal Care and Use Committee.

TABLE I
SPECIMEN PARAMETERS AND TEST CONDITIONS

Subject ID	Head Length (cm)	Head Width (cm)	Mass (kg)	Peak Incident Overpressure (kPa)	Duration (ms)	Apnea	Brain Haemorrhage Grade	Survival Time (hr)
16	7.0	5.3	1.0	287	2.8	Yes	Mild	5
17	7.0	5.5	0.9	327	3.2	Yes	Severe	0.28
25	8.0	6.0	1.1	225	2.2	No	Moderate	5
26	7.5	6.5	0.9	291	2.6	Yes	Severe	1.5
41	7.5	6.0	1.4	234	0.71	No	None	5
45	8.0	6.5	1.2	335	0.75	No	None	5
46	8.0	6.0	1.1	320	0.75	No	Mild	5
Control								
67	8.0	7.0	1.4	NA	NA	No	None	5

The ferrets were exposed to a simulated free-field blast from an 20.32-cm diameter shock tube, described in [46]. As significant pulmonary injury occurs at lower peak pressures than severe brain injury, and thoracic protection can decrease the blast threat [15][46-48], the thorax and abdomen were protected in a steel tube with attenuating foam placed in the openings. To reduce global head motion from the blast wind, the head and neck were supported and secured on a 12.7-cm-long head support extended from the protective cylinder. The head support and protective fixture weighed 24.86 kg. The head was secured to the support using a high tensile strength, waterproof and oil resistant medical tape (Kendall Wet Pruf ® Tape, Covidian, Mansfield, MA, USA). The centre of the head of the specimen was placed approximately 3.81 cm from the opening of the shock tube. The head support fixture allowed limited movement and limited blast protective capabilities to decrease the likelihood of the securing techniques themselves causing head injury. A Kevlar (DuPont Co., Wilmington, DE, USA) collar was also placed around the neck of the specimens to prevent neck motion and injury. High-speed video (Redlake HG-100K, Tallahassee, FL, USA or Phantom v5.0, Wayne, NJ, USA) was taken to examine the amount of

the head motion present in each test.

Specimens were euthanised following the procedures detailed in [45], five hours after exposure unless the clinical condition after the blast deteriorated despite resuscitation efforts. After perfusion fixation, the brains were immersed in 0.1M phosphate buffer containing 4% paraformaldehyde (Electron Microscopy Sciences, Hatfield, PA, USA) at 4°C for 16 hours. They were then placed in 0.1 M phosphate buffer containing 20% sucrose also at 4°C. The sucrose solution was replaced the following day. The brains were shipped in the second sucrose solution within seven days of extraction to FD Neurotechnologies, Inc. (Baltimore, MD, USA), where the brains were rapidly frozen and stored at -75°C.

Calculating Head Kinematics

High-speed video of the exposure event was captured at 1024 x 1024 pixels at 8 bit color resolution at 1,000 frames per second. The vertex of the head and a fixed point on the support fixture were tracked manually. The relative distance between these points was used to obtain the kinematics. Due to space restrictions within the test set-up, these points were not perpendicular to the optical axis of the camera, nor were these points along the direction of motion. However, the scaling of objects that did not move, but were in the same plane as the points within the images for the different tests remained constant. Furthermore, the images were scaled using objects with known dimensions near the tracked points to make sure the measured pixels between images were equivalent. Therefore, the relative motions between tests could be compared, but not absolute motions.

The relative distance between the head and the support fixture was normalised by subtracting the initial distance between the two points before the event and any motion had occurred from all subsequent measurements. The velocity was calculated by differentiating via a second order central difference approximation of the displacement-time history. The acceleration was determined by taking a second order central difference approximation of the velocity.

Immunohistochemical Labelling of Brain Tissue

Serial sections were cut coronally on a cryostat through the whole cerebrum (approximately corresponding to the rat brain from bregma 5.64 mm to -9.00 mm, cf. [49]). Every 1st through 7th section of each series of 25 sections (interval: 1.0 mm, thickness: 40 μm) was collected separately in section storage solution, to be processed according to the procedures outlined below. In addition, serial sections (two sections per set, seven sets per brain) were also collected from the brainstem and the cerebellum approximately at the levels corresponding to the rat bregma,-10.20 mm and -10.80 mm, respectively. All free-floating sections were stored at -20°C before further processing.

The sections of the 2nd set were processed for RM014 (clone: RM014.9, Invitrogen, Carlsbad, CA, USA, Cat. #34-1000). To begin, the sections were incubated free-floating in 0.01 M phosphate-buffered saline (PBS, pH 7.4) containing 1% normal horse serum (Vector Lab., Burlingame, CA, USA), 0.3% Triton X-100 (Sigma, St. Louis, MO, USA) and the mouse anti-neurofilament antibody (1:500) for 42 hours at 4°C after inactivating the endogenous peroxidase activity with hydrogen peroxidase. Next, the immunoreaction product was visualised according to the avidin-biotin complex (ABC) method from [50] with the Vectastin elite ABC kit (Vector Lab., Burlingame, CA, USA). The sections were incubated in PBS containing biotinylated horse anti-mouse immunoglobin G (IgG), Triton-X and normal horse serum for one hour, and then in PBS containing avidin-biotinylated horseradish peroxidase complex for another hour. This was followed by incubation of the sections for three minutes in 0.05 M Tris buffer (pH 7.2) containing 0.03% 3',3'-diaminobenzidine (Sigma, St. Louis, MO, USA) and 0.0075% H_2O_2. All steps were carried out at room temperature, except as indicated, and each step was followed by washes in PBS. After thorough rinses in distilled water, all sections were mounted on slides, dehydrated in ethanol, cleared in xylene and coverslipped in Permount® (Fisher Scientific, Fair Lawn, NJ, USA).

The sections of the 3rd set were processed for β-APP in the following manner. The sections were placed in 0.1 M citric buffer (pH 6.0) and microwaved at 45°C for five minutes after inactivating the endogenous peroxidase activity with hydrogen peroxidase. Following 20 minutes of cooling at room temperature, sections were pre-incubated for 40 minutes in 0.01 M PBS (pH 7.4) containing 10% normal goat serum (NGS, Vector Lab., Burlingame, CA, USA) and 0.3% Triton X-100 (Sigma, St. Louis, MO). Sections were then incubated for 42 hours at 4°C in PBS containing 1% NGS and the rabbit anti-C-terminus of the human β-APP (1:2,000, Invitrogen, Carlsbad, CA, USA, Cat. #51-2700). Next, the immunoreaction product was visualised according to the avidin-biotin complex method from [50] with the Vectastin elite ABC kit (Vector Lab., Burlingame, CA, USA) similar to the RM014

procedure. The sections were incubated in PBS containing a biotinylated goat anti-rabbit IgG, Triton-X and NGS for one hour and then in PBS containing an avidin-biotinylated horseradish peroxidase complex for another hour. This was followed by incubation of the sections for four minutes in 0.05 M Tris buffer (pH 7.2) containing 0.03% 3',3'-diaminobenzidine (Sigma, St. Louis, MO, USA) and 0.0075% H_2O_2. After thorough rinses in distilled water, sections were mounted on microscope slides, dehydrated in ethanol, cleared in xylene and coverslipped in Permount® (Fisher Scientific, Fair Lawn, NJ, USA).

Analysis of Immunohistochemical Findings

The slides were first viewed under light microscopy and then digitally scanned at 40X magnification using an Aperio ScanScope CS slide scanning system (Aperio Technologies, Inc., Vista, CA, USA). The digitised histological slides were further evaluated to quantify the amount of positive staining present. As immunohistochemistry is based on enzyme-linked immunoreactivity, it can be quantitative, similar to enzyme-linked immunosorbent assay (ELISA) tests [51]. Previous studies have quantified immunohistochemistry by using segmentation or thresholding of grayscale or colour images [52]. A similar technique was used in this analysis.

Quantitative analysis was performed on 1700 x 1080 µm sections of the internal capsule, a deep subcortical structure that contains a high concentration of motor and sensory white matter projection fibers. Although the sections of tissue were only labelled with one antibody, similar sections of tissue from the same specimen were stained with the other antibody to investigate the co-localisation of the two different types of injured axons.This methodology cannot identify whether the same axon has immunoreactivity to both IHC labels; however, it can identify the regions of the brain that are more or less reactive to the different labels. The location of the slices that contained the analysed portion of the internal capsule was approximately -4.6 mm from bregma. MATLAB® (2013a, The MathWorks, Natick, MA, USA) code was used to identify positive immunoreactivity based on pixel colour and region size and shape because including region size and shape produces more reliable results than colour or intensity alone [53].

For RM014, the contrast of each RGB component (red, green, blue) was optimised to reduce the amount of background in the image. A threshold was determined for each component image using Otsu's method [54] with some modifications to account for background staining. The thresholds within the same colour component were within 3% for all of the images. Regions within the image that had an area between 5 and 1000 µm and possessed a linear shape were identified as immunopositive axons. Each component of the RGB colour model was analysed separately following this method, and then unique regions that were identified in the components were added together to determine the total area of immunopositive axons within each section of brain tissue.

For β-APP, the threshold was determined using just the red component of the RGB colour model. Again, the thresholds for all of the images were within 3% of one another. The axons that demonstrated positive staining for β-APP within this region of the brain for these exposure conditions were punctate in appearance. Consequently, the area limits for immunopositive axons were between 1 and 20 µm. This antibody also displayed immunoreactivity within the blood vessels in the brain. Additional code was written to identify blood vessels by altering the threshold to increase the area of each identified blood vessel, so that area and linear shape could be used to remove them from the selected regions.

Statistical Analyses

The quantitative histological results were analysed using JMP software (JMP®, Version 12.0.1. SAS Institute Inc., Cary, NC 1989-2015). A paired t-test was conducted to compare the amount of immunopositivity using the IHC label for RM014 and β-APP. To examine the relationship between the amount of positive staining for each marker and the magnitude of loading for the two injury mechanisms (shock wave and acceleration) separate linear regression models were used. As blast brain injury has been shown to be dependent on overpressure and duration [45], a pseudo-impulse of the pressure conditions was calculated by multiplying the peak incident overpressure and the duration and dividing the result by two. Although pressure data was collected for all of the tests, only a subset of those traces were available to analyze for this study. To keep the methodology consistent for all of the specimens, this pseudo-impulse was used instead of directly calculating the impulse from the pressure traces. The dependent variables, areas of positive staining for each IHC label, were normalised using the controls so that the area of positive staining would be zero if no exposure occurred, using Eq. 1:

$$IHC_{scaled} = \frac{(IHC_i - IHC_0)\times 10}{IHC_{\max} - IHC_0}, \quad (1)$$

where IHC_{scaled} is the normalized area for the IHC label, IHC_i is the measured IHC area for the i^{th} subject (μm^2), IHC_0 is the IHC area for the control (μm^2), and IHC_{max} is the IHC area for the subject with the greatest amount of staining (μm^2). The independent variables, relative head acceleration and impulse, were then transformed so each variable was on a scale from 0 to 10, using Eq. 2:

$$x_{scaled} = \frac{(x_i - 0)\times 10}{x_{\max} - 0} \quad (2)$$

where x_{scaled} is the scaled variable, x_i is the value of the variable for the i^{th} subject, and x_{max} is the value of the variable for the subject with the greatest value. This transformation was done so that the slopes of the lines could be more easily compared.

III. RESULTS

In addition to the blast overpressure exposure, the seven ferrets had a range of global head motion. Table II provides the relative head accelerations of the ferrets. Two of the seven ferrets died before the full five-hour time course of the study. Three of the seven ferrets experienced a period of apnea after the blast exposure, including the two that died prematurely. Five ferrets displayed some degree of haemorrhage on the surface of the brain.

TABLE II
HEAD KINEMATICS, BLAST CONDITIONS, QUANTITATIVE IMMUNOHISTOCHEMISTRY

Subject ID	Relative Head Acceleration (Test/Lowest Acc Test)	Peak Incident Overpressure (kPa)	Duration (ms)	Area of Positive Staining – RM014 (μm^2)	Area of Positive Staining – β-APP (μm^2)
16	2.579524	287	2.8	41549	34
17	2.391953	327	3.2	36689	28
25	3.07649	225	2.2	39988	21
26	2.713929	291	2.6	56919	54
41	1	234	0.71	29902	17
45	1.576128	335	0.75	25177	7
46	1.60318	320	0.75	21264	6
Control					
67	NA	NA	NA	11014	0

Neurofilament Alteration Following Blast Exposure

Examination using immunohistochemistry specific for RM014 revealed positive staining in multiple white matter fiber pathways, including the internal and external capsules, the thalamic pathways, the cerebral and cerebellar peduncles, the optical tracts, trapezoid body, and pyramids (Fig. 1 A–F). However, the intensity and frequency of staining in the commissural fibers, such as the corpus callosum, were not as great as other large white matter fiber tracts (Fig. 1F). Evidence of neurofilament alterations was seen even in the specimens that did not survive the full five hours post-exposure (Fig. 1H), as well as in the un-blasted specimen (Fig. 1I). When the RM014 antibody binds to the epitope of the neurofilament sidearm, a secondary antibody is used to react with the primary antibody to reveal a darkened colour. The secondary antibody can also bind to non-specific targets, leading to background staining. The high relative intensity of the stain, the location of the stain (i.e. areas in the brain where axons would be located), and the morphology of the stained areas (i.e. linear and punctate morphologies) were used to identify positively stained axons. The intensity and number of positively stained axons appeared to increase with increased blast severity (Fig. 1G).

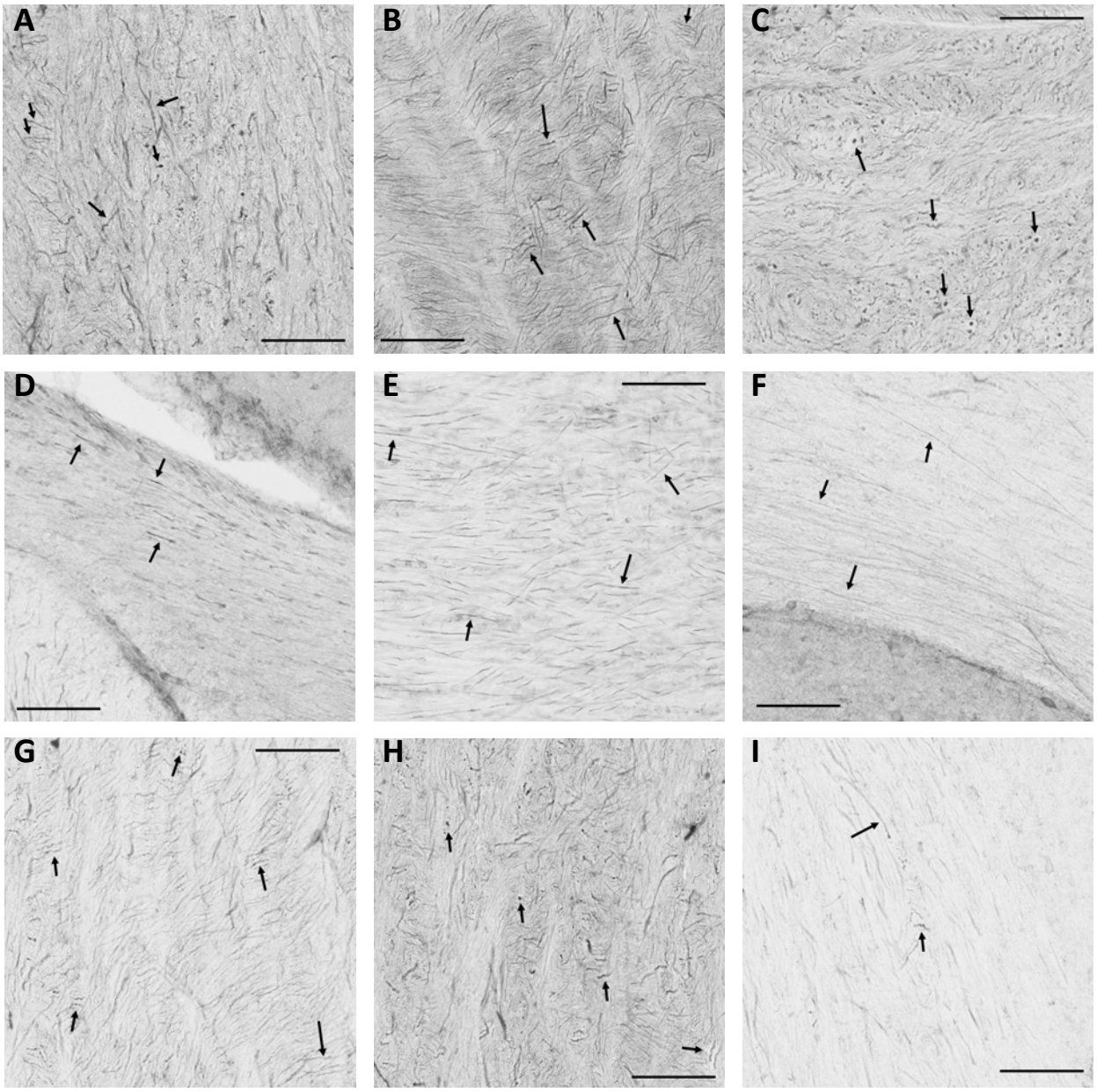

Fig. 1. Some examples of positive immunoreactivity for neurofilament alteration using antibodies for RM014 are identified (*arrows*) in ferrets exposed to primary blast. The scale bar for all images is 100 µm.
A. Internal capsule from Subject 25 (specimen with the highest relative acceleration and moderate impulse).
B. Thalamic pathway from Subject 25.
C. Cerebellar peduncle from Subject 25.
D. Optical tract from Subject 25.
E. Trapezoid body from Subject 25.
F. Corpus callosum from Subject 25.
G. Internal capsule from Subject 41 (specimen with the lowest relative acceleration and impulse). The intensity of staining (*darkness*) and number of positive areas are not as high as Subject 25.
H. Internal capsule from Subject 17 (specimen with short survival time).
I. Internal capsule from Subject 67 (control, i.e. no blast exposure). The intensity of staining is not as high for the control as for the blasted specimens.

Microtubule Alteration Following Blast Exposure via Impaired Axonal Transport Visualisation

Examination using immunohistochemistry specific for β-APP revealed positive staining in the blasted specimens

throughout the cerebrum and brainstem. The positively stained axons were generally isolated and surrounded by uninjured axons, but were sometimes found in a cluster. Some common areas of positive staining included: the corpus callosum, the internal and external capsules, the hippocampus, the thalamus, the cerebellum, the optical tracts, trapezoid body, and pyramids, cortical grey-white interface, and near the borders of ventricles (Fig. 2 A–F). Evidence of impaired axonal transport was seen even in the specimens that did not survive the full five hours post-exposure (Fig. 2H). Much like the RM014 IHC label, background staining was visible for the β-APP label. The high relative intensity of the stain, the location of the stain (i.e. areas in the brain where axons would be located), and the morphology of the stained areas (i.e. linear with spheroid area, demonstrating a comet-like appearance and punctate morphologies) were used to identify positively stained axons. The intensity, size and number of positively stained axons appeared to increase with increased blast severity (Fig. 2G).

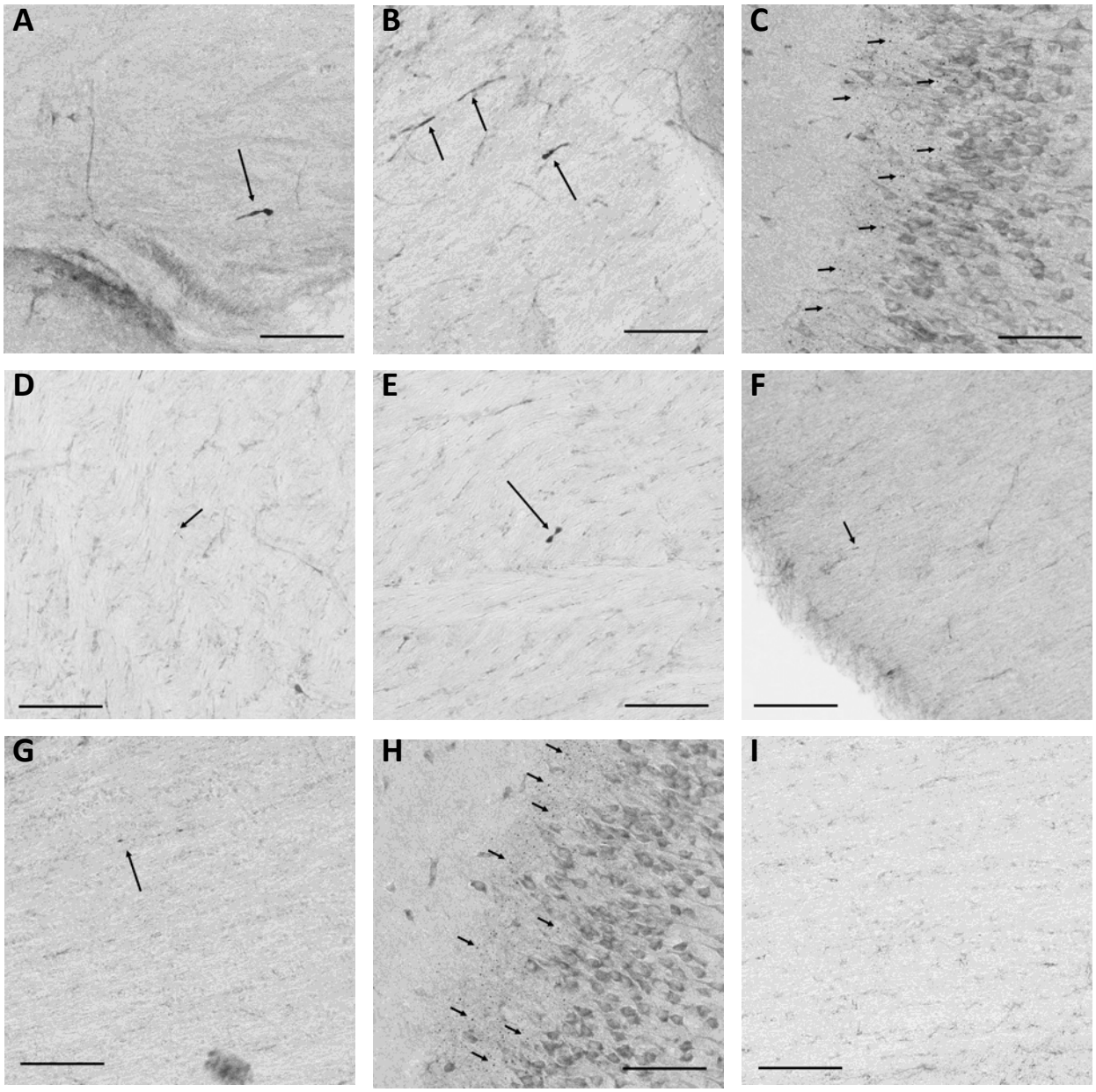

Fig. 2. Some examples of positive immunoreactivity for impaired axonal transport using antibodies for β-APP are identified (*arrows*) in ferrets exposed to primary blast. The scale bar for all images is 100 µm.
A. Corpus callosum from Subject 25 (specimen with the highest relative acceleration and moderate impulse).
B. Internal capsule from Subject 25.
C. Hippocampus from Subject 25. The positive staining in this region demonstrated a punctate morphology.
D. Thalamic pathway from Subject 25.

E. Cerebellar peduncle from Subject 25.
F. Near border of lateral ventricle from Subject 25.
G. Corpus callosum from Subject 41 (specimen with the lowest relative acceleration and impulse). The size of the positively stained area is smaller than the specimen exposed to a higher blast loading condition.
H. Hippocampus from Subject 17 (specimen with short survival time).
I. Corpus callosum from Subject 67 (control, i.e. no blast exposure). There were no positive axons identified in this region.

Statistical Results

The paired t-test showed that the two IHC labels did not positively stain the same amount of tissue within the analysed section of the internal capsule. The difference in the positively stained area was significant for RM014 (M=35926.9, SD=11945.78) and β-APP (M=23.9, SD=16.8); $t(6)=-7.96$, $p<0.001$. These results suggest that an early time after blast exposure, within this section of the brain there is more neurofilament alteration than fully impaired axonal transport.

The regression analysis revealed that the specimen with the shortest survival time, 17 minutes, was an outlier. Previous studies support the omission of this case from further analysis considering biological processes necessary to visualise the axonal injury markers require some time to occur. RM014 has been seen as early as 30 minutes, and β-APP has been visualized 1 hr after brain injury [32][55], but this specimen did not survive as long as either of those timepoints. For pseudo-impulse, the slopes of the lines for the two IHC labels are similar. For head acceleration, the slope of the line for RM014 is steeper than the line for β-APP by 9%.

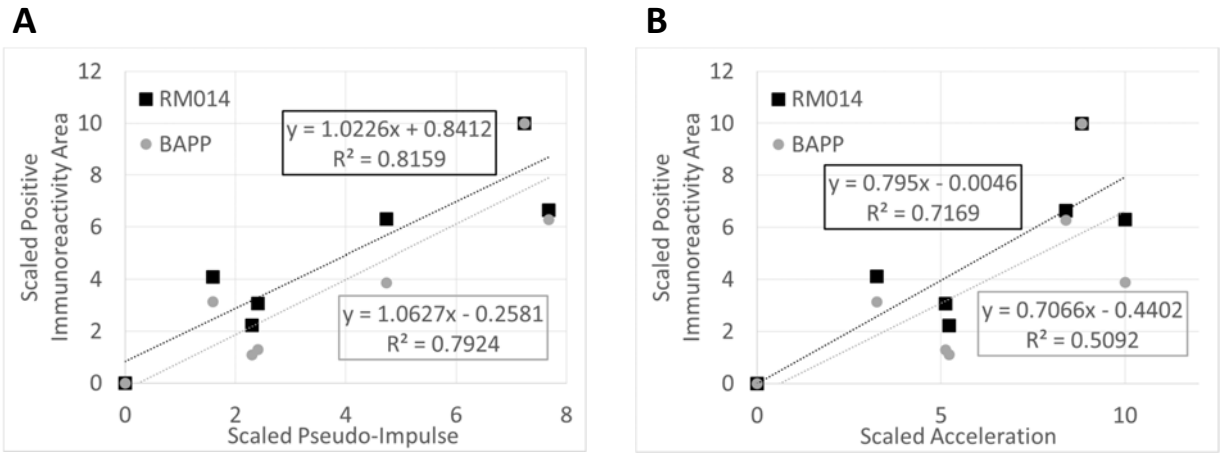

Fig. 3. Graphs of the immunohistochemical labels and the blast parameters. The linear regression analysis is also displayed on the charts. The box outlined in black corresponds to the RM014 linear fit, and the box outlined in grey corresponds to β-APP.
A. The relationship between the IHC markers and pseudo-impulse.
B. The relationship between the IHC markers and head acceleration.

IV. Discussion

The immunoreactivity of the two IHC labels differed in amount and location in the brain. In general for the loading conditions in this study, more locations in the brain were immunopositive for impaired axonal transport than axons with altered neurofilaments. Although, the overall area of positive staining was greater for axons with altered neurofilaments. The areas with β-APP positive axons also did not always correspond to the areas of RM014 positive axons. One explanation for this observation may be that the composition of axons is not uniform and depends on axon caliber. In other words, smaller axons contain more microtubules per unit area, whereas larger axons contain more neurofilaments per unit area [31][56]. For example, the hippocampus had extensive staining for β-APP, but no positive staining for RM014. The axons within the hippocampus are of a smaller caliber, so they would be more likely to show damaged axonal transport than neurofilament alteration [57]. RM014 positive staining was more prevalent than β-APP in the peduncular region of the cerebrum and cerebellum. The axons in

the peduncular regions are some of the largest in the brain and therefore have more neurofilaments per unit area than other regions in the brain [58].

Another explanation for the differences in the amount of staining may be the survival time after the exposure. Neurofilament alteration can occur from direct mechanical loading, such as axonal stretching and shearing of the cytoskeletal elements [59-60]. β-APP is detected where fast axonal transport is disrupted, and takes time to accumulate at the site of disruption to be visualised [19][61]. Although immunoreactivity has been seen as early as six hours after blast exposure in other studies, the amount of positive staining increases for at least 18 hours after exposure [35]. The five-hour survival time used in this study is early in the time window in which β-APP detection occurs. Furthermore, two of the specimens did not survive the full five hours. It is possible that should more time have elapsed between exposure and sacrifice, the amount of positive staining for β-APP would be more similar to RM014.

While the relationship between the staining and blast exposure is the most likely cause for the immunoreactivity patterns in the tissue, artifacts from tissue preparation cannot be excluded. The specimens were sacrificed prior to the perfusion fixation procedures. Although the animals were administered heparinised saline prior to euthanasia, and the perfusion procedures began as soon as the euthanasia solution was injected, poor perfusion of the fixative could have occurred. Poor perfusion can contribute to autolysis of the tissue, increasing the phosphatase activity, thus increasing the staining pattern for RM014 [61]. β-APP immunoreactivity may also have been affected by the euthanasia and perfusion fixation procedures, as it has been shown to be immunoreactive as a result of hypoxic conditions [61].Furthermore, peroxidase-based IHC is highly sensitive to sample preparation and processing. Although the same procedures were followed for all of the sections, not all of the sections were processed at the same time in the same development solution. Hence, some of the variation may be due to some samples being processed at different times. Finally, positive staining does not necessarily indicate brain injury since disruptions in axonal transport and neurofilament alterations can result from numerous causes.

Error in the immunohistochemistry analysis could also be introduced in the quantification algorithms. Some of the analysed images had large variances in the background intensities. Typical global thresholding techniques can be affected by large variances in background intensities. Even though a modified technique was used to address this issue, because the threshold was not the same for all images, the quantification of positive immunoreactivity between specimens may have additional error.

In this study, RM014 positive staining was extensive throughout entire sections of brain tissue. In previous studies of TBI utilising the IHC label for RM014, the axons stained positively in a more isolated fashion [31][37][56][63]. This staining pattern indicates that the injury in this model is different than traditional TBI [31][56]. The immunoreactivity of the β-APP label also differed from traditional TBI. The β-APP positive axons stained diffusely throughout the brain, which is in contrast to traditional TBI where the injured axons are generally found on the ipsilateral side [41-42]. However, this finding is similar to another study of blast brain injury where there appeared to be no regional difference of positive staining [35]. Many other brain injury biomarkers that have been used in blast studies have also not demonstrated a regional dependence [10][15][18][64-68]. However, not all reported biomarkers for blast brain injury lack regional specificity. For example, another marker for neurofilament injury is more prevalent on the ipsilateral side to the blast exposure [33], as are markers for apoptotic transcriptional factors [35][69].

The regression models for the two immunohistochemical labels did not demonstrate a different dependence on the impulse injury mechanism in the internal capsule of brain tissue; however, a difference was seen with regards to the acceleration. The positive immunoreactivity of RM014 appears to be more affected by acceleration than β-APP. As stated before, there are more neurofilaments in large caliber axons, and large caliber axons span across different regions of the brain. Greater accelerations may result in higher differential movement in the various brain regions, perhaps introducing an additional shearing load on the large caliber axons. The high frequency content of blast waves may affect smaller scales of tissue than automotive brain injury. Brain injury resulting from automotive impacts are often attributed to angular acceleration. The differential movement that is considered one of the injury mechanisms for angular accelerations, may also contribute to the injury mechanism from accelerations due to blast. Despite this differential relationship to acceleration, the slopes of the lines for the impulse fits were greater than the slopes for the acceleration fits for both IHC labels indicating that the impulse may play a larger role in the response of the IHC labels under a blast exposure.

In addition to the previous limitations mentioned for the IHC labels, the regression models are also affected by the limitations in the calculations of the two analysed injury mechanisms. Errors in the acceleration can be introduced by out-of-plane motion and pixel size. Since the camera was not positioned directly perpendicular to the primary direction of movement, out-of-plane motion may have a larger contribution to the error. However, in this study, the field of view of the camera was large enough such that the error in out-of-plane motion is not larger than the error in pixel size considering the dimensions of the objects within the same plane of the tracked points in motion did not significantly change during the duration of measurements. Because not all of the pressure traces were available for this study, the impulse had to be estimated using a simplified approximation, knowing that impulse is related to the peak pressure and overpressure duration of the pressure wave. However, this simplified approximation may not accurately reflect the actual impulses that were witnessed.

V. CONCLUSIONS

Exposure to primary blast resulted in brain injury in a ferret model. Axonal injury was demonstrated using markers for neurofilament alteration and impaired axonal transport. The immunoreactivity of the two IHC labels differed in amount and location in the brain. The amount of immunoreactivity for RM014 was more dependent on the amount of head acceleration than β-APP. Although the true contributions of impulse and acceleration to the immunoreactivity of the IHC labels cannot be determined from this study, the different relationships between RM014 and β-APP and head acceleration warrant further study to understand all of the mechanisms of blast brain injury.

VI. REFERENCES

[1] Zuckerman, S. (1941) Discussion on the Problem of Blast Injuries. *Proc R Soc of Med,* **34**: pp.171–88.

[2] Phillips, Y. Y. (1986) Primary Blast Injuries. *Ann Emer Med,* **15**(12): pp.1446–50.

[3] Clemedson, C. J., Pettersson, H. (1956) Propagation of a high explosive air shock wave through different parts of an animal body. *Am J Physiol,* **184**(1): pp.119–126.

[4] Chavko, M., Koller, W. A., Prusaczyk, W. K., McCarron, R. M. (2007) Measurement of blast wave by a miniature fiber optic pressure transducer in the rat brain. *J Neurosci Methods,* **159**(2): pp.277–81.

[5] Saljo, A., Arrhen, F., Bolouri, H., Mayorga, M., Hamberger, A. (2008) Neuropathology and pressure in the pig brain resulting from low-impulse noise exposure. *J Neurotrauma,* **25**(12): pp.1397–1406.

[6] Bauman, R. A., Ling, G. *et al*. (2009) An introductory characterization of a combat-casualty-care relevant swine model of closed head injury resulting from exposure to explosive blast. *J Neurotrauma,* **26**(6): 841–60.

[7] Nyein, M. K., Jason, A. M. *et al*. (2010) In silico investigation of intracranial blast mitigation with relevance to military traumatic brain injury. *Proc Natl Acad Sci,* **107**(48): pp.20703–8.

[8] Chavko, M., Watanabe, T. *et al*. (2011) Relationship between orientation to a blast and pressure wave propagation inside the rat brain. *J Neurosci Methods,* **195**(1): pp.61–6.

[9] Dal Cengio Leonardi, A., Bir, C. A., Ritzel, D. V., VandeVord, P. J. (2011) Intracranial pressure increases during exposure to a shock wave. *J Neurotrauma,* **28**(1): pp.85–94.

[10] Svetlov, S. I., Prima, V. *et al*. (2010) Morphologic and biochemical characterization of brain injury in a model of controlled blast overpressure exposure. *J Trauma Inj Infect Crit Care,* **69**(4): pp.795–804.

[11] Sundaramurthy, A., Alai, A. *et al*. (2012) Blast-induced biomechanical loading of the rat: an experimental and anatomically accurate computational blast injury model. *J Neurotrauma,* **29**(13): pp.2352–64.

[12] Adams, J. H., Graham, D. I., Gennarelli, T. A., Maxwell, W. L. (1991) Diffuse axonal injury in non-missile head injury. *J Neurol Neurosurg Psychiatry,* **54**(6): pp.481–3.

[13] Petras, J. M., Bauman, R. A., Elsayed, N. M. (1997) Visual system degeneration induced by blast overpressure. *Toxicology,* **121**(1): pp.41–9.

[14] Cernak, I., Wang, Z., Jiang, J., Bian, X., Savic, J. (2001) Cognitive deficits following blast-injury induced neurotrauma: possible involvement of nitric oxide. *Brain Inj,* **15**(7): pp.593–612.

[15]Long, J. B., Bentley, T. L. *et al*. (2009) Blast overpressure in rats: recreating a battlefield injury in the laboratory. *J Neurotrauma,* **26**(6): pp.827–40.

[16] Cheng, J., Gu, J. *et al*. (2010) Development of a rat model for studying blast-induced traumatic brain injury. *J Neurol Sci,* **294**(1-2): pp.23–8.

[17] Garman, R., Jenkins, L. W. *et al*. (2011) Blast exposure in rats with body shielding is characterized by diffuse axonal injury. *J Neurotrauma,* **28**(6): pp.947–59.

[18] Koliatsos, V. E., Cernak, I. *et al*. (2011) A mouse model of blast injury to brain: initial pathological, neuropathological, and behavioral characterization. *J Neuropathol Exp Neurol,* **70**(5): pp.399–416.

[19] de Lanerolle, N. C., Bandak, F. *et al*. (2011) Characteristics of an explosive blast-induced brain injury in an experimental model. *J Neuropathol Exp Neurol,* **70**(11): pp.1046–57.

[20] Lu, J., Ng, K.C. *et al*. (2012) Effect of blast exposure on the brain structure and cognition in *Macaca fascicularis*. *J Neurotrauma,* **29**(7): pp.1434–54.

[21] Smith, D. H., Meaney, D. F. (2000) Axonal damage in traumatic brain injury. *Neuroscientist,* **6**(6): pp.483–95.

[22] Ransom, B. R. (2003) Medical Physiology: A Cellular and Molecular Approach, pp.257–79. *Saunders,* Philadelphia, USA.

[23] Christman, C. W., Grady, M. S., Walker, S. A., Holloway, K. L., Povlishock, J. T. (1994) Ultrastructural studies of diffuse axonal injury in humans. *J Neurotrauma,* **11**(2): pp.173–86.

[24] Maxwell, W. L., Graham, D. I. (1997) Loss of axonal microtubules and neurofilaments after stretch-injury to guinea pig optic nerve fibers. *J Neurotrauma,* **14**(9): pp.603–14.

[25] Jafari, S. S., Maxwell, W. L., Neilson, M., Graham, D. I. (1997) Axonal cytoskeletal changes after non-disruptive axonal injury. *J Neurocytol,* **26**(4): pp.201–21.

[26] Jafari, S. S., Nielson, M., Graham, D. I., Maxwell, W. L. (1998) Axonal cytoskeletal changes after nondisruptive axonal injury. II. Intermediate sized axons. *J Neurotrauma,* **15**(11): pp.955–66.

[27] Maxwell, W. L., Domleo, A., McGoll, G., Jafari, S. S., Graham, D. I. (2003) Post-acute alterations in the axonal cytoskeleton after traumatic axonal injury. *J Neurotrauma,* **20**(2): pp.151–68.

[28] Serbest, G., Burkhardt, M. F., Siman, R., Raghupathi, R., Saatman, K. E. (2007) Temporal profiles of cytoskeletal protein loss following traumatic axonal injury in mice. *Neurochem Res,* **32**(12): pp.2006–14.

[29] Tang-Schomer, M. D., Patel, A. R., Baas, P. W., Smith, D. H. (2010) Mechanical breaking of microtubules in axons during dynamic stretch injury underlies delayed elasticity, microtubule disassembly, and axon degeneration. *FASEB J,* **24**(5): pp.1401–10.

[30] Johnson, V. E., Stewart, W., Smith, D. H. (2012) Axonal pathology in traumatic brain injury. *Exp Neurol,* **246**: pp.35–43.

[31] Stone, J. R., Singleton, R. H., Povlishock, J. T. (2001) Intra-axonal neurofilament compaction does not evoke local axonal swelling in all traumatically injured axons. *Exp Neurol,* **172**: pp.320–31.

[32] DiLeonardi, A. M., Huh, J. W., Raghupathi, R. Impaired axonal transport and neurofilament compaction occur in separate populations of injured axons following diffuse brain injury in the immature rat. *Brain Res,* **1263**: pp.174–82.

[33] Saljo, A., Bao, F., Haglid, K. G., Hansson, H. A. (2000) Blast exposure redistribution of phosphorylated neurofilament subunits in neurons of the adult rat brain. *J Neurotrauma,* **17**(8): pp.719–26.

[34] Kallakuri, S., Purkait, H. S., Dalavayi, S., VandeVord, P., Cavanaugh, J. M. (2015) Blast overpressure induced axonal injury changes in rat brainstem and spinal cord. *J Neurosci Rural Pract,* **6**(4): pp.481–7.

[35] Saljo, A., Bao, F. *et al*. (2002) Expression of c-Fos and c-Myc and deposition of β-APP in neurons in the adult rat brain as a result of exposure to short-lasting impulse noise. *J Neurotrauma,* **19**(3): pp.379–85.

[36] Buki, A., Siman, R., Trojanowski, J. Q., Povlishock, J. T. (1999) The role of calpain-mediated spectrin proteolysis in traumatically induced axonal injury. *J Neuropathol Exp Neurol,* **58**(4): pp.365–75.

[37] Marmarou, C. R., Walker, S. A., Davis, C. L., Povlishock, J. T. (2005) Quantitative analysis of the relationship between intra-axonal neurofilament compaction and impaired axonal transport following diffuse traumatic brain injury. *J Neurotrauma,* **22**(10): pp.1066–80.

[38] Bain, A. C., Raghupathi, R., Meaney, D. F. (2001) Dynamic stretch correlates to both morphological abnormalities and electrophysiological impairment in a model of traumatic axonal injury. *J Neurotrauma,* **18**(5): pp.499–511.

[39] Medana, I. M., Esiri, M. M. (2003) Axonal damage: a key predictor of outcome in human CNS diseases. *Brain,* **126**(Pt 3): pp.515–30.

[40] McKenzie, K. J., McLellan. D. R. *et al*. (1996) Is β-APP a marker of axonal damage in short-surviving head injury? *Acta Neuropathol*, **92**(6): pp.608–13.

[41] Pierce, J. E. S., Trojanowski, J. Q., Graham, D. I., Smith, D. H., McIntosh, T. K. (1996) Immunohistochemical

characterization of alterations in the distribution of amyloid precursor proteins and β-amyloid peptide after experimental brain injury in the rat. *J Neurosci*, **16**(3): pp.1083–90.

[42] Bramlett, H. M., Kraydieh, S., Green, E. J., Dietrich, W. D. (1997) Temporal and regional patterns of axonal damage following traumatic brain injury: a β-amyloid precursor protein immunocytochemical study in rats. *J Neuropathol Exp Neurol*, **56**(10): pp.1132–41.

[43] Stone, J. R., Singleton, R. H., Povlishock, J. T. (2000) Antibodies to the C-terminus of the β-amyloid precursor protein (APP): a site specific marker for the detection of traumatic axonal injury. *Brain Res*, **871**(2): pp.288–302.

[44] Ai, J., Liu, E., Park, E., Baker, A. J. (2007) Structural and functional alterations of cerebellum following fluid percussion injury in rats. *Exp Brain Res*, **177**(1): pp.95–112.

[45] Rafaels, K. A., Bass, C. R. *et al*. (2012) Brain injury risk from primary blast. *J Trauma Acute Care Surg,* **73**(4): pp.895–901.

[46] Rafaels, K., Bass, C.R. *et al*. (2011) Survival risk assessment for primary blast exposures to the head. *J Neurotrauma,* **28**(11): pp.2319–28.

[47] Hooker, D. R. (1924) Physiological Effects of Air Concussion. *Am J Physiol*, **67**: pp.219–74.

[48] Wood, G. W., Panzer, M. B., Shridharani, J. K., Matthews, K. A., Bass, C. R. Attenuation of blast overpressure behind ballistic protective vests. *Proceedings of Personal Armour Systems Symposium*, 2010, Quebec City, Canada.

[49] Paxinos, G., Watson, C. (2007) Rat Brain in Stereotaxic Coordinates. *Academic Press,* London, UK.

[50] Hsu, S. M., Raine, L., Fanger, H. (1981) Use of avidin-biotin-peroxidase complex (ABC) in immunoperoxidase techniques: a comparison between ABC and unlabeled antibody (PAP) procedures. *J Histochem Cytochem,* **29**: pp.577–80.

[51] Taylor, C. R., Levenson, R. M. (2006) Quantification of immunohistochemistry – issues concerning methods, utility and semiquantitative assessment II. *Histopathology*, **49**(4): pp.411–24.

[52] Matkowskyj, K. A., Schonfeld, D., Benya, R. V. (2000) Quantitative immunohistochemistry by measuring cumulative signal strength using commercially available software Photoshop and MATLAB. *J Histochem Cytochem*, **48**(2): pp.303–12.

[53] Rojo, M. G., Bueno, G., Slodkowska, J. (2009) Review of imaging solutions for integrated quantitative immunohistochemistry in the pathology daily practice. *Folia Histochem Cytobiol*, **47**(3): pp.349–54.

[54] Otsu, N. A. (1979) Threshold Selection Methodfrom Gray-Level Histograms. *IEEE Transactions on Systems, Man, and Cybernetics,* **9**(1): pp.62–6.

[55]Pierce, J. E., Trojanowski, J. Q., Graham, D. I., Smith, D. H., & McIntosh, T. K. (1996) Immunohistochemical characterization of alterations in the distribution of amyloid precursor proteins and beta-amyloid peptide after experimental brain injury in the rat. *Journal of Neurosci*, ***16***(3), pp.1083-90.

[56] Marmarou, C. R., Povlishock, J. T. (2006) Administration of the immunophilin ligand FK506 differentially attenuates neurofilament compaction and impaired axonal transport in injured axons following diffuse traumatic brain injury. *Exp Neurol*, **197**(2): pp.353–62.

[57] Papasozomenos, S. C., Binder, L. I. (1987) Phosphorylation determines two distinct species of Tau in the central nervous system. *Cell Motil Cytoskeleton*, **8**(3): pp.210–26.

[58] Watson, D. (1991) Regional variation in the abundance of axonal cytoskeletal proteins. *J Neurosci Res*, **30**(1): pp.226–31.

[59] Pal, J., Toth, Z. *et al*. (2006) Selective induction of ultrastructural (neurofilament) compaction in axons by means of a new head-injury apparatus. *J Neurosci Methods*, **153**(2): pp.283–9.

[60] Siedler, D. G., Chuah, M. I., Kirkcaldie, M. T. K., Vickers, J. C., King, A. E. (2014) Diffuse axonal injury in brain trauma: insights from alterations in neurofilaments. *Front Cell Neurosci,* **8**: p.429.

[61] Geddes, J. F., Whitwell, H. L., Graham, D. I. (2000) Traumatic axonal injury: practical issues for diagnosis in medicolegal cases. *Neuropath Appl Neurobio,* **26**(2): pp.105–16.

[62] Scudamore, C. L., Hodgson, H. K. *et al*. (2011) The effect of post-mortem delay on immunohistochemical labelling – a short review. *Comp Clin Pathol,* **20**(2): pp.95–101.

[63] Stone, J. R., Okonkwo, D. O. *et al*. (2004) Impaired axonal transport and altered axolemmal permeability occur in distinct populations of damaged axons following traumatic brain injury. *Exp Neurol*, **190**(1): pp.59–69.

[64] Kaur, C., Singh, J. *et al*. (1995) The response of neurons and microglia to blast injury in the rat brain. *Neuropathol Appl Neurobiol*, **21**(5): pp.369–77.

[65] Kaur, C., Singh, J. *et al.* (1996) Studies of the choroid plexus and its associated epiplexus cells in the lateral ventricles of rats following an exposure to a single non-penetrative blast. *Arch Histol Cytol,* **59**(3): pp.239–48.

[66] Kaur, C., Singh, J., Lim, M. K., Ng, B. L., Ling, E. A. (1997) Macrophages/microglia as 'sensors' of injury in the pineal gland of rats following a non-penetrative blast. *Neurosci Res*, **27**(4): pp.317–22.

[67] Saljo, A., Bao, F., Hamberger, A., Haglid, K. G., Hansson, H. A. (2001) Exposure to short-lasting impulse noise causes microglial and astroglial cell activation in the adult rat brain. *Pathophysiology*, **8**(2): pp.105–11.

[68] Saljo, A., Huang, Y. L., Hansson, H. A. (2003) Impulse noise transiently increased the permeability of nerve and glial cell membranes, an effect accentuated by a recent brain injury. *J Neurotrauma*, **20**(8): pp.787–94.

[69] Kato, K., Fujimura, M. *et al*. (2007) Pressure-dependent effect of shock waves on rat brain: induction of neuronal apoptosis mediated by a caspase-dependent pathway. *J Neurosurg*, **106**(4): pp.667–76.